Supporting Information

Regulating the donor number of solvents for long-cycle anode-free lithium metal batteries

Yining Zhao, Shaopeng Li, Lingtong Zhu, Yahui Li, Shu Xu, Hui Dou, and Xiaogang Zhang*

Jiangsu Key Laboratory of Materials and Technologies for Energy Storage, College of Material Science and Technology, Nanjing University of Aeronautics and Astronautics, Nanjing 211100

*Corresponding Author: Xiaogang Zhang: azhangxg@nuaa.edu.cn

1. Experimental Section

1.1 Chemicals and reagents

Lithium bis(fluorosulfonyl)imide (LiFSI) and lithium nitrate ($LiNO_3$) were purchased from Alfa Aesar. 1,1,2,2-tetrafluoroethyl 2,2,3,3-tetrafluoropropyl ether (TTE) and tetraethylene glycol dimethyl ether (G4) were purchased from Duoduo chemical reagent Co., Ltd. Conventional commercial carbonate-based electrolyte (1.0 M $LiPF_6$/EC-DMC (1:1 vol%)-30%FEC) was purchased directly from Shanshan Advanced Materials (Quzhou) Co., Ltd.

1.2 Battery Fabrication and Electrochemical Measurements

The NCM622 positive electrode consisted of 80 wt% NCM622 powder, 10 wt% acetylene black, and 10 wt% PVDF with an active material loading of about 17.67 mg cm^{-2}. The electrode was punched into a circle with a diameter of 10 mm. Lithium chips were purchased from Tianjin Zhong Neng Corporation. Battery assembly and disassembly were performed in an argon-filled glove box (H_2O and O_2 content < 0.01 ppm) using a CR-2016 type button cell case with a single piece of Celgard 2500 separator and 30 μL electrolyte injected on each side of the diaphragm. A Land Instruments Battery Tester was used for the cycling performance measurements. EIS was performed with ZIVE SP2 electrochemical instruments (WonATech Co, LTD), the perturbation amplitude was 10 mV, and the operating frequency ranged from 1×10^5 Hz to 1×10^{-2} Hz.

1.3 Materials Characterization

The *in-situ* observation of the Li depositing process was conducted with an optical microscope and ChenHua CHI760 system. The *in-situ* optical observation unit is supported by the Beijing Scistar Technology Co. Ltd. ^{7}Li NMR (AVANCE NEO 400M) and Raman spectrometer (LabRAM HR Evolution) were carried out to detect the evolution of Li^+-solvation structure and identify the electrolyte components. The ^{7}Li NMR spectra were referenced to the signal of 0.1 M LiCl in D_2O (0 ppm). Li metal anodes and NCM622 cathodes, after predesigned cycles, were cleaned with DMC to wipe off the remaining lithium salts and electrolytes. The morphologies of samples were investigated by scanning electron microscopy (Scios 2 HiVac) and high-resolution transmission electron microscopy (Talos F200X G2). To prepare the samples, the cycled samples were washed several times with dimethyl carbonate (DMC) in an Ar-filled glovebox (H_2O/O_2 <0.1 ppm) to remove the residual electrolyte, and then dried under vacuum and stored in airtight containers. For TEM analysis, cross-sectional FIB milling was performed using a Thermo Fisher Scientific Scios2 HiVac focused ion beam-scanning electron microscope (FIB-SEM) system. 2.2 mm thick Pt layer was firstly deposited on the particles to be lifted out to avoid Ga-ion-beam damage. Afterward, the specimen was thinned to electron transparency using 30 kV Ga-ion beam. A final polishing using 2 kV Ga ion was performed to reduce the surface damage layer. The samples were transferred to the TEM sample bars using a specially designed vacuum-sealed transfer device. The surface chemistry of cycled electrodes was analyzed by XPS (ESCALAB Xi+, Thermo Fisher) and TOF-SIMS (LYRA3 TESCAN). Energy dispersive spectrum (EDS) was conducted to characterize the transition metal distribution and redeposition in a certain area.

1.4 Theoretical Methods

In this work, MD simulations were performed to elucidate the effect of the diluent (TTE) on the solvated structure. The MD simulations were performed using the software package GROMACS (version 2021.3).[1-4] Molecules were first optimized using ORCA. The system was constructed by packmol,[5] and composed of specific molecules in a cubic box with an edge size of 5 nm. The atomic interactions were parameterized by the optimized potentials for liquid simulations all-atom (OPLS-AA) force field,[6] and RESP2 charge obtained from Multiwfn[7] was applied in the calculations. After the energy minimization, the systems were pre-balanced in the NPT ensemble with the Berendsen method for 1 ns. Then, the production run was carried out in the NPT ensemble at 300 K with the time step of 1 fs. The temperature of the system was controlled by a V-rescale thermostat (τT = 1 ps) and the pressure was controlled by the Parrinello-Rahman method (τP = 2 ps). After 20 ns of simulation, the RDF of the particles was analyzed by the toolkits of GROMACS.

All electronic structure calculations were performed using the ORCA (version 5.0.4) software package. ORCA is a versatile quantum chemistry program capable of performing various types of calculations, including density functional theory (DFT), Hartree-Fock (HF), and post-HF methods. Geometry optimizations were carried out using the B97-3C functional with the embedded basis set. Single-point energy calculations were performed using RI-B3LYP-D3 (BJ) function with the larger def2-TZVP basis set to obtain accurate electronic energies. To account for dispersion interactions, the DFT-D3 correlation correction was included in the calculations. This correction accounts for the long-range dispersion forces that are not adequately captured by standard DFT functionals. The D3 correction was applied with the Becke-Johnson damping scheme.[8, 9] The desolvation energy Edesolvation of Li^+-(solvent)$_x$ complexes were calculated with the equation (1) below:

$$E_{desolvation} = E_{Li^+-solvent} - x \times E_{solvent} - E_{Li^+} \qquad (1)$$

where $E_{Li^+-solvent}$ represents the total energy of the solvent interacting with a single Li^+, $E_{solvent}$ is the energy of the solvent, and E_{Li^+} is the energy of a single Li^+.

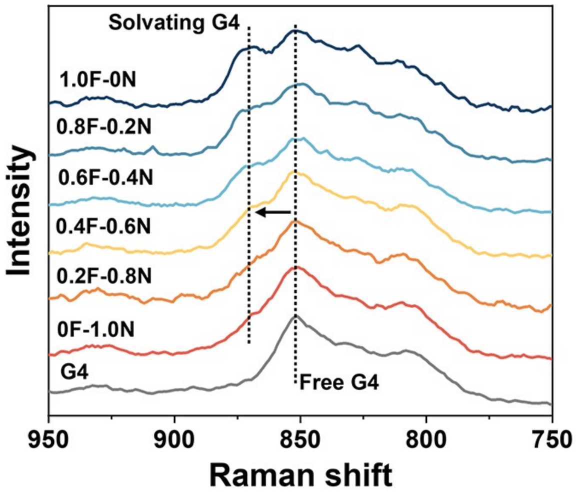

Figure S1. Raman spectra of varying the molar ratio of LiFSI:$LiNO_3$ in G4 in the 1 M electrolytes.

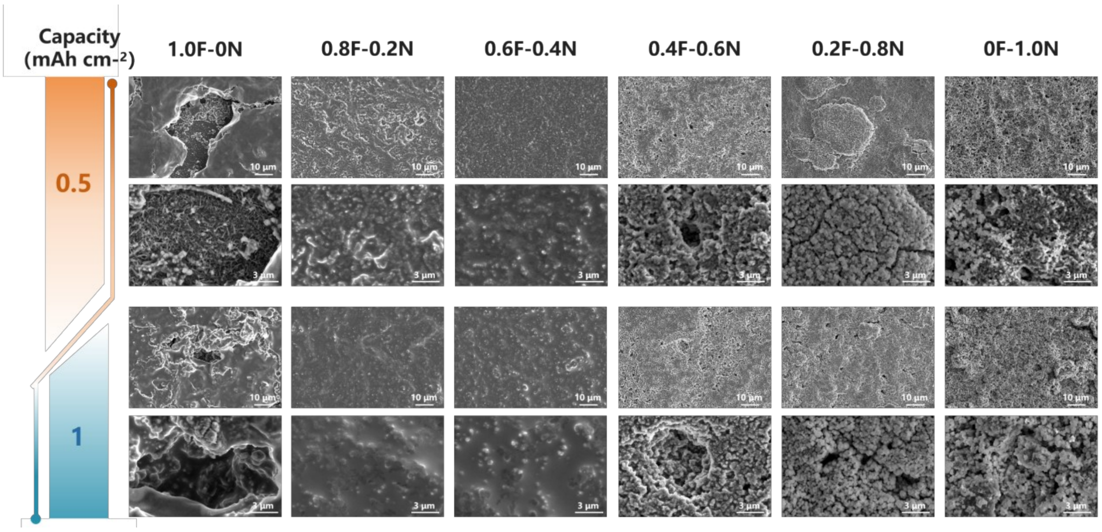

Figure S2. SEM images of Li electrodeposits obtained in the 1 M electrolytes with varied molar ratios of LiFSI:$LiNO_3$ in G4.

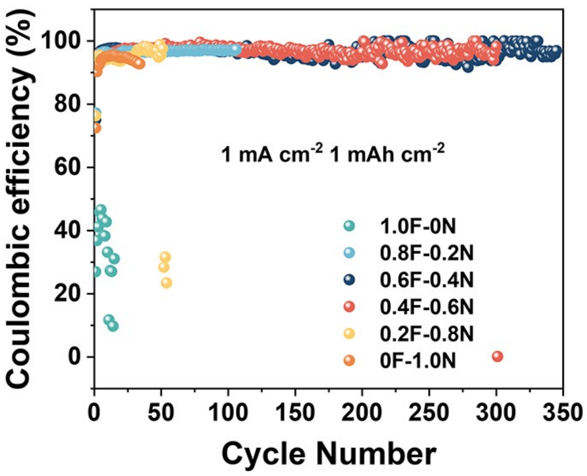

Figure S3. Li metal plating/stripping CEs evaluated by Li||Cu half cells at 1 mA cm^{-2} with a fixed discharge capacity of 1 mAh cm^{-2}.

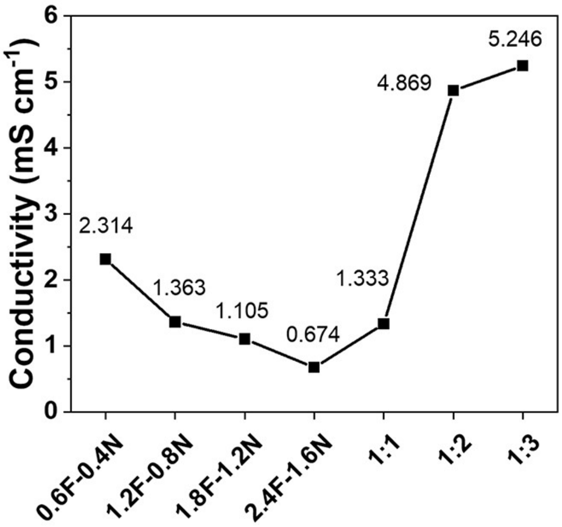

Figure S4. Ionic conductivity of different electrolytes.

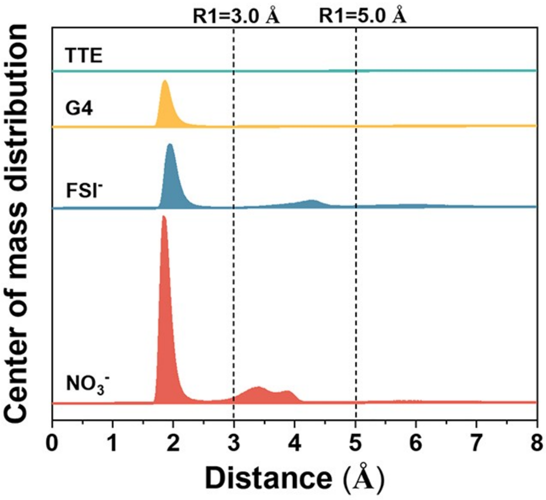

Figure S5. CM distribution of given NO_3^-, FSI^-, G4 and TTE for 2.4F-1.6N-TTE.

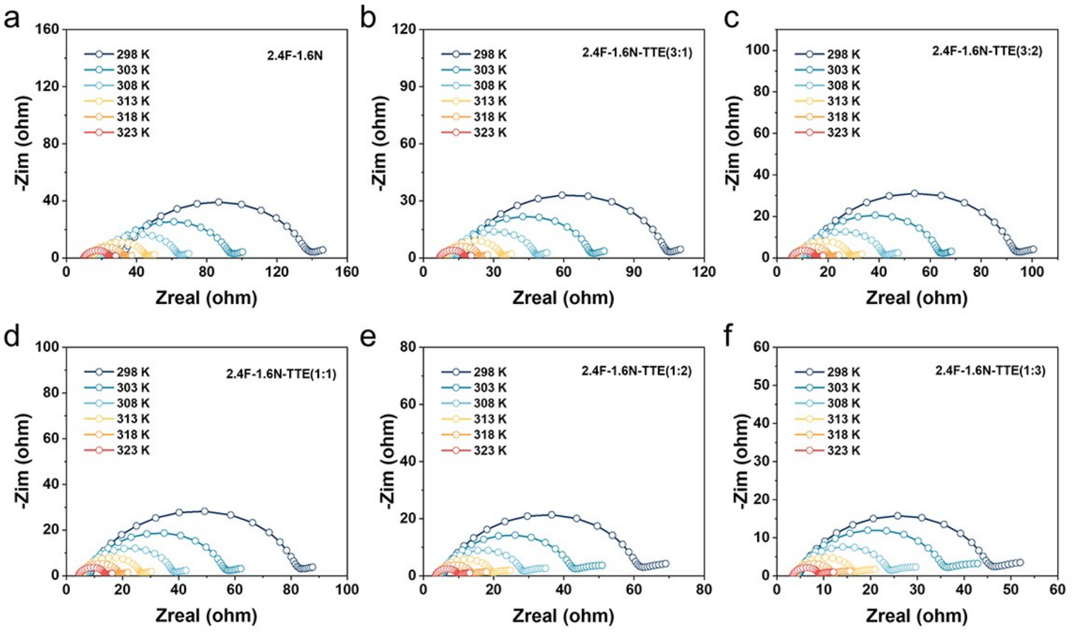

Figure S6. Nyquist plots of Li||Li symmetric cells in different electrolytes with varied volume ratios of 2.4F-1.6N:TTE at temperatures from 298 K to 323 K after 5 cycles at 0.5 mA cm^{-2} with a plating amount of 1.0 mAh cm^{-2}.

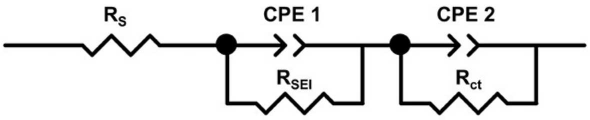

Temperature (K)	R_{ct} （Ω）					
	2.4F-1.6N	3:1	3:2	1:1	1:2	1:3
298	37.33	19.08	18.49	19.12	17.44	15.02
303	27.70	12.36	16.46	17.32	13.60	12.06
308	17.40	10.08	10.21	13.71	10.22	8.97
313	11.16	7.08	8.24	8.23	8.51	7.92
318	10.42	6.49	6.69	5.68	6.69	6.50
323	6.74	5.99	5.86	4.76	6.25	5.29

Figure S7. The equivalent circuit for the temperature-dependent EIS and fitting results.

The temperature-dependent EIS spectra is fitted according to the equivalent circuit diagram and the fitting result is shown above. The fitted results were brought into the Arrhenius equation to obtain the activation energies for Li^+ desolvation (E_{ct}) at the anode interface:

$$\kappa = \frac{T}{R_{ct}} = A\exp\left(-\frac{E_{ct}}{RT}\right)$$

where κ is the rate constant of the reaction, T is the absolute temperature, R_{ct} is the charge transfer resistance, A is the preexponential constant and R is the standard gas constant.

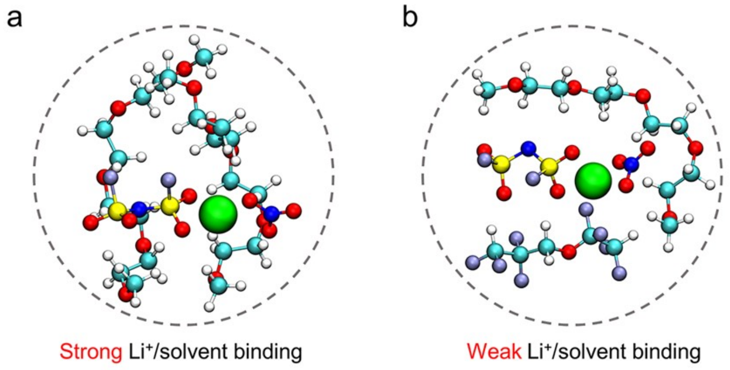

Figure S8. Most probable solvation structure extracted from MD simulation for (a) 2.4F-1.6N and (b) 2.4F-1.6N-TTE electrolytes.

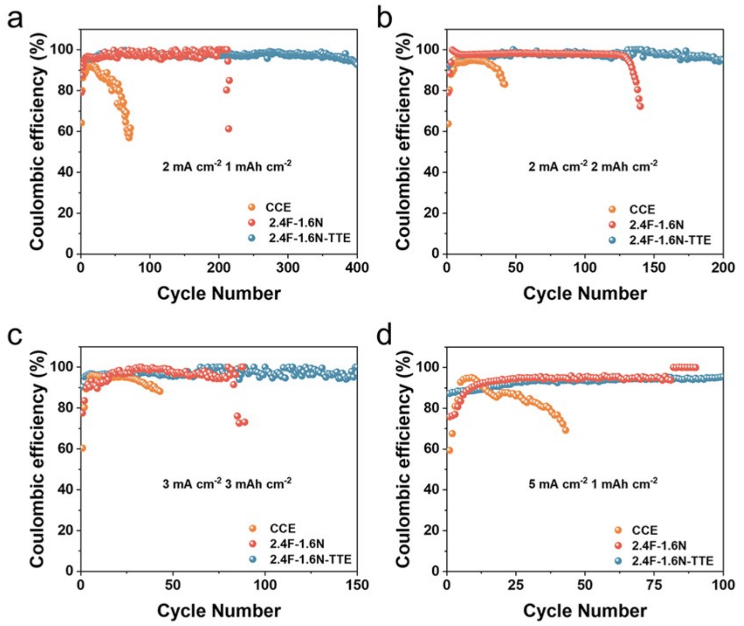

Figure S9. Li metal plating/stripping CEs evaluated by Li||Cu half cells at various current densities and capacities: (a) 2 mA cm^{-2}/ 1 mAh cm^{-2}, (b) 2 mA cm^{-2}/ 2 mAh cm^{-2}, (c) 3 mA cm^{-2}/ 3 mAh cm^{-2} and (d) 5 mA cm^{-2}/ 1 mAh cm^{-2}.

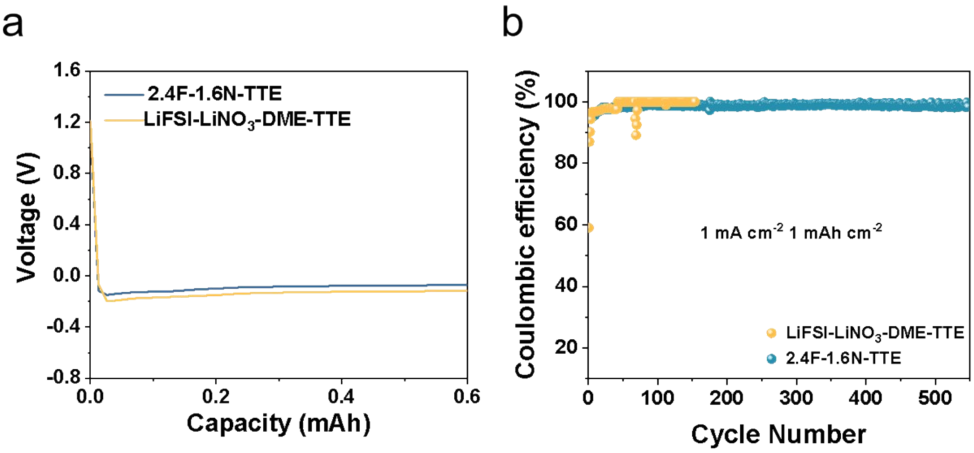

Figure S10. (a) Corresponding voltage-capacity profiles during the first cycle using different electrolytes. (b) The CE of Li metal plating and stripping was assessed using Li||Cu half cells at 1 mA cm^{-2} for 1 mAh cm^{-2}.

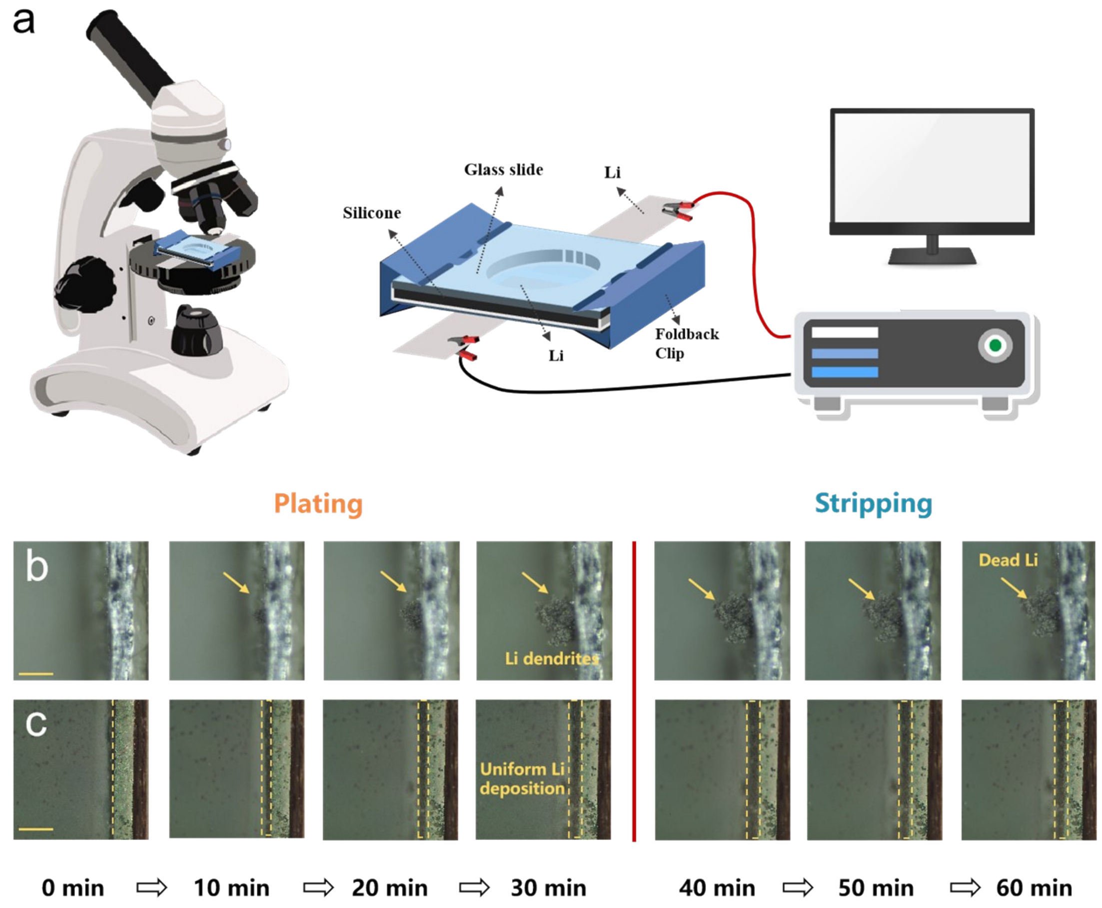

Figure S11. (a) Schematic diagram of in-situ optical observation device. In situ optical microscopy observation of the Li deposition process in (b) CCE and (c) 2.4F-1.6N-TTE at 5 mA cm^{-2} and 5 mAh cm^{-2}, the ruler is 200 μm.

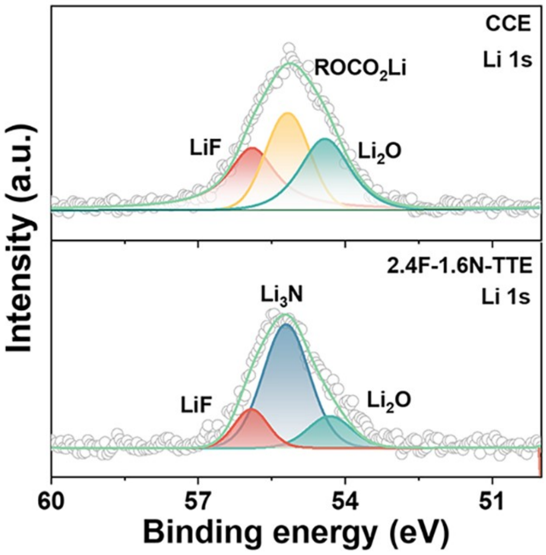

Figure S12. XPS spectra of Li1s on the Li-metal anode at 0.5 mA cm^{-2}, 0.5 mAh cm^{-2} after 10 cycles.

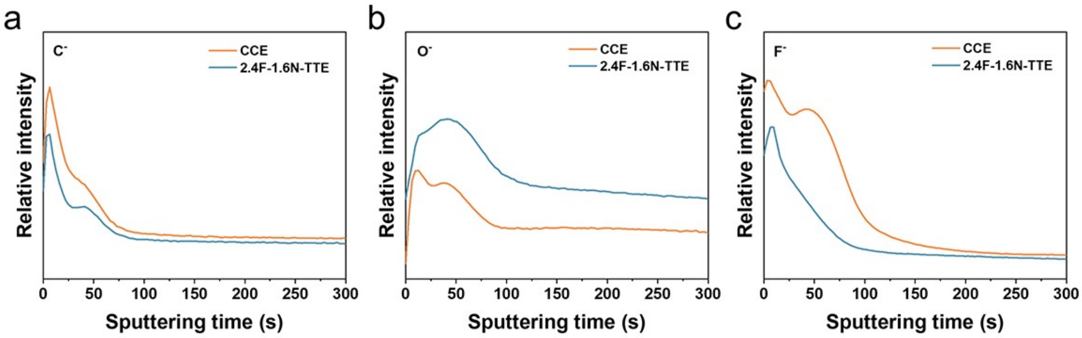

Figure S13. Relative intensity of (a) C$^-$, (b) O$^-$ and (c) F$^-$ in the CCE and 2.4F-1.6N-TTE.

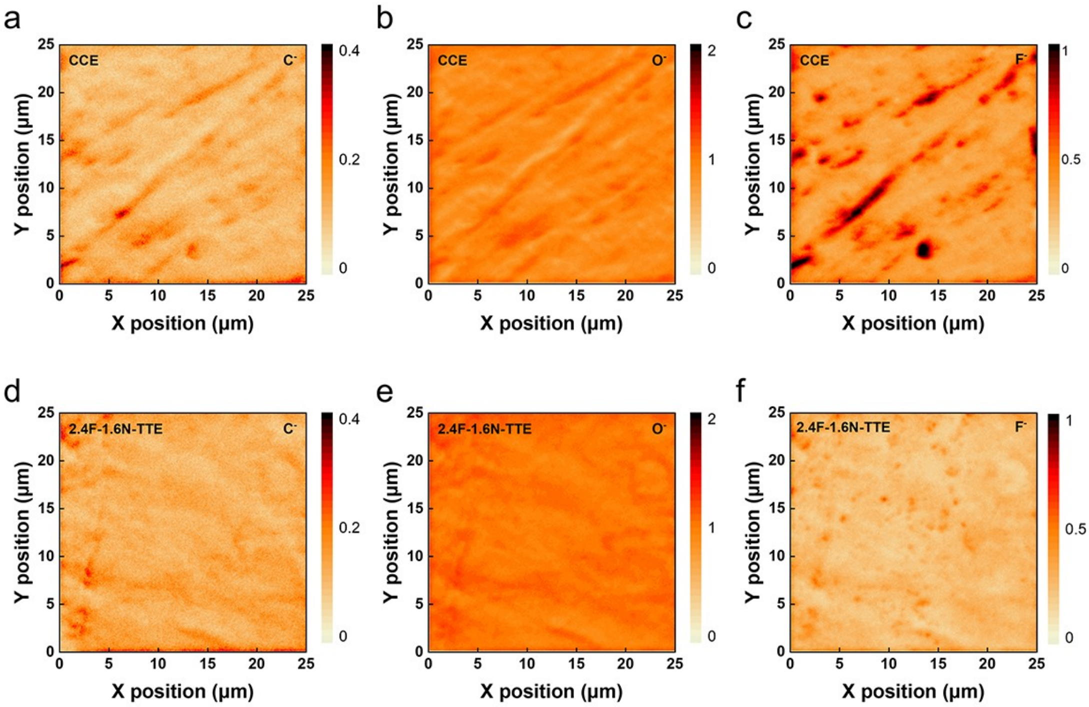

Figure S14. Surface TOF-SIMS component mapping on Li metal anodes. (a) C⁻, (b) O⁻ and (c) F⁻ in the CCE. (d) C⁻, (e) O⁻ and (f) F⁻ in the 2.4F-1.6N-TTE.

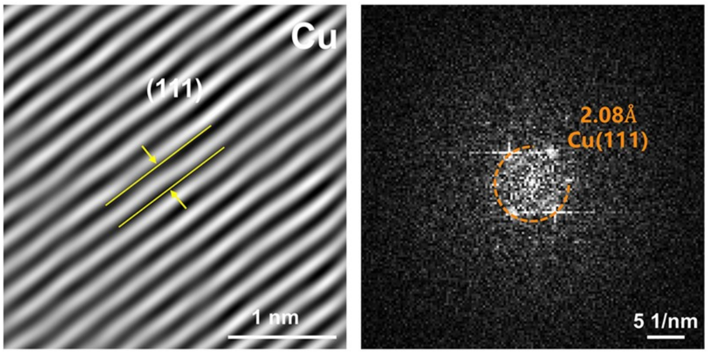

Figure S15. The fast Fourier transform images of Cu.

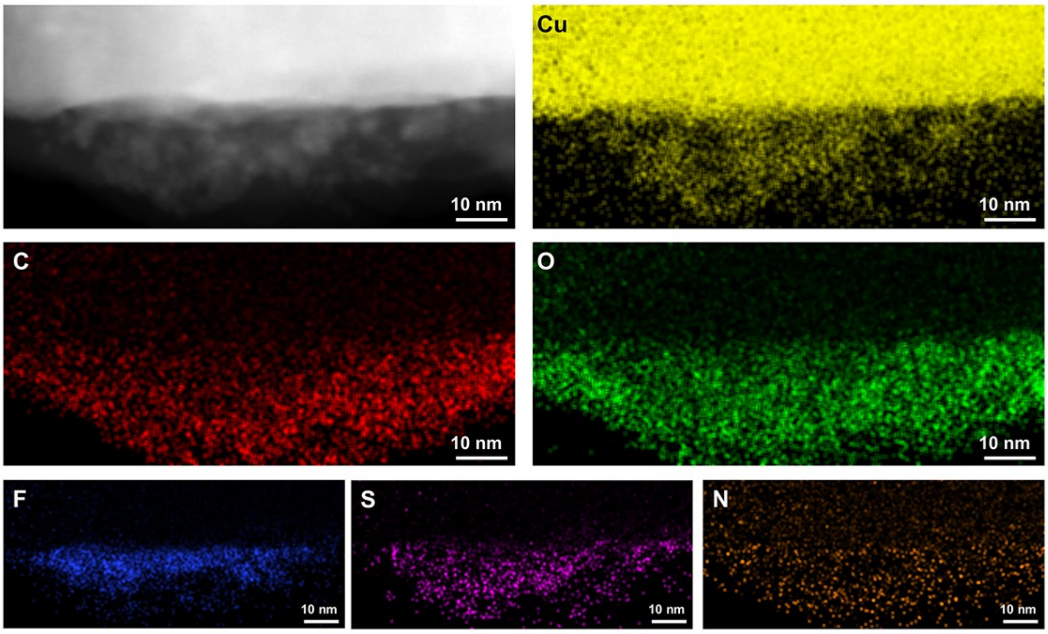

Figure S16. HRTEM image of SEI and EDS elemental mappings of the Cu, C, O, F, S and N elements.

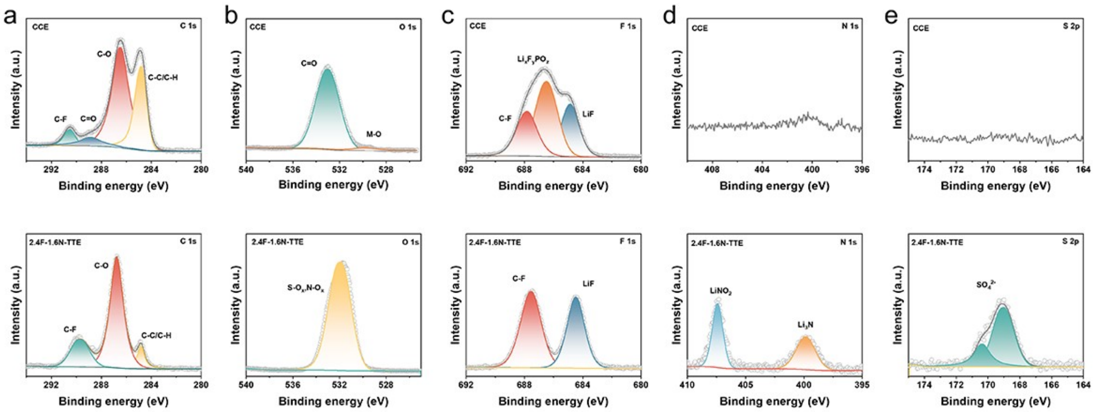

Figure S17. XPS characterization of the CEI components on cycled NCM622. (a) C_{1s}, (b) O_{1s}, (c) F_{1s}, (d) N_{1s}, (e) S_{2p}.

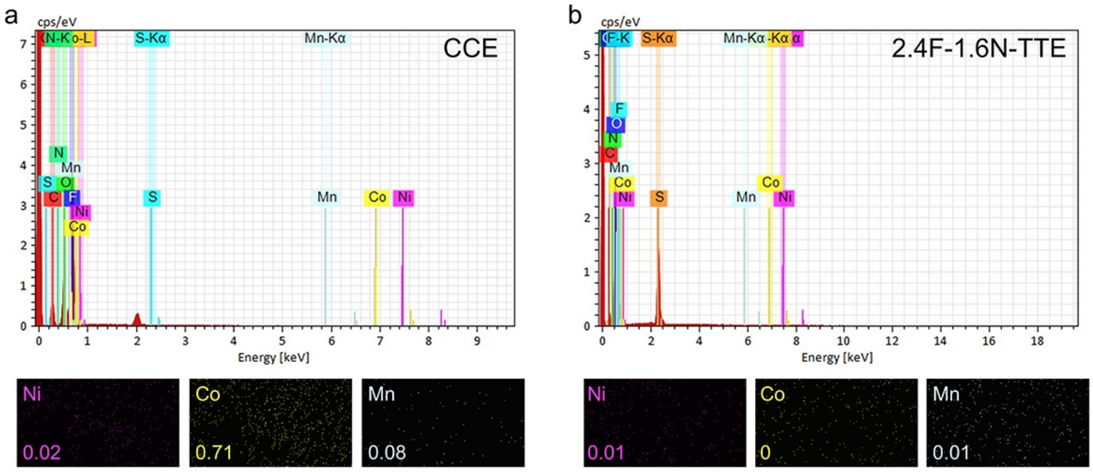

Figure S18. EDS and corresponding transition metal element mapping performed on dismantled Li anodes after 100 cycles in Li||NCM622 cells with (a) CCE and (b) 2.4F-1.6N-TTE.

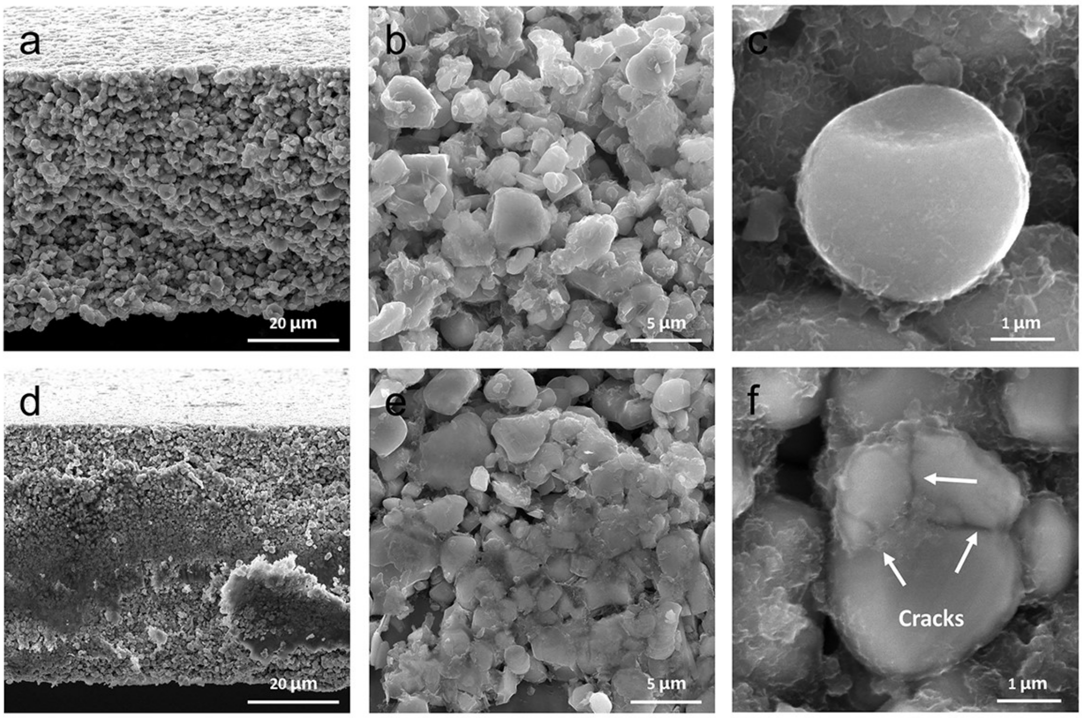

Figure S19. Cross-sectional SEM images of NCM622 particles cycled in (a-c) 2.4F-1.6N-TTE and (d-f) CCE based electrolyte after 110 cycles at 0.5 C.

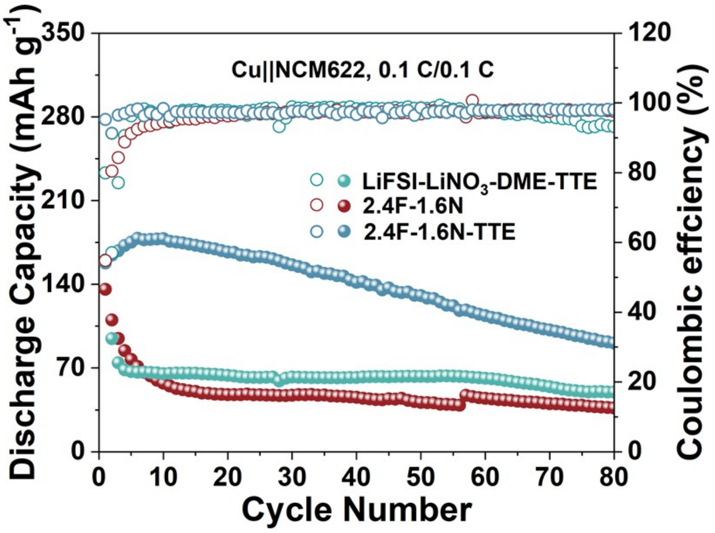

Figure S20. Cycling performance of NCM622||Cu cells using different electrolytes.

Reference

1. Van Der Spoel, D.; Lindahl, E.; Hess, B.; Groenhof, G.; Mark, A. E.; Berendsen, H. J. C. Gromacs: Fast, Flexible, and Free. *J. Comput. Chem.* **2005**, *26*, 1701-1718.
2. Páll, S.; Abraham, M. J.; Kutzner, C.; Hess, B.; Lindahl, E. Tackling Exascale Software Challenges in Molecular Dynamics Simulations with Gromacs. *Solving Software Challenges for Exascale* **2015**, *8759*, 3-27.
3. Abraham, M. J.; Murtola, T.; Schulz, R.; Páll, S.; Smith, J. C.; Hess, B.; Lindahl, E. J. S. Gromacs: High Performance Molecular Simulations through Multi-Level Parallelism from Laptops to Supercomputers. *SoftwareX* **2015**, *1*, 19-25.
4. Berendsen, H. J.; van der Spoel, D.; van Drunen, R. J. C. p. c. Gromacs: A Message-Passing Parallel Molecular Dynamics Implementation. *Comput. Phys. Commun.* **1995**, *91*, 43-56.
5. Martínez, L.; Andrade, R.; Birgin, E. G.; Martínez, J. M. Packmol: A Package for Building Initial Configurations for Molecular Dynamics Simulations. *J. Comput. Chem.* **2009**, *30*, 2157-2164.
6. Jorgensen, W. L.; Maxwell, D. S.; Tirado-Rives, J. Development and Testing of the Opls All-Atom Force Field on Conformational Energetics and Properties of Organic Liquids. J. *Am. Chem. Soc.* **1996**, *118*, 11225-11236.
7. Lu, T.; Chen, F. Multiwfn: A Multifunctional Wavefunction Analyzer. *J. Comput. Chem.* **2012**, *33*, 580-592.
8. Neese, F. Software Update: The Orca Program System—Version 5.0. *Wiley Interdisciplinary Reviews: Computational Molecular Science* **2022**, *12*, e1606.
9. Grimme, S.; Antony, J.; Ehrlich, S.; Krieg, H. A Consistent and Accurate AB Initio Parametrization of Density Functional Dispersion Correction (DFT-D) for the 94 Elements H-

Pu. *J. Chem. Phys.* **2010**, *132*, 154104.